Identification of a nitrogen vacancy in GaN by scanning probe microscopy

Keisuke Sagisaka,[1,2,*] Oscar Custance,[1,2] Nobuyuki Ishida,[1,2] Tomonori Nakamura,[1] and Yasuo Koide[1,3]

[1]*Center for GaN Characterization and Analysis, National Institute for Materials Science, 1-2-1 Tsukuba, Ibaraki 305-0047, Japan*

[2]*Research Center for Advanced Measurement and Characterization, National Institute for Materials Science, 1-2-1 Tsukuba, Ibaraki 305-0047, Japan*

[3]*Research Center for Functional Materials, National Institute for Materials Science, 1-2-1 Tsukuba, Ibaraki 305-0047, Japan*

(Received 19 June 2022; accepted 12 September 2022; published 29 September 2022)

Gallium nitride (GaN) is a material with important applications in optoelectronics, wireless communications, and power electronics. Devices for such applications are normally made with GaN single-crystal wafers. Yet an infinitesimal amount of atomic defects in these single crystals considerably hinders the electronic performance of GaN. One kind of atomic defect in GaN crystals that has been theoretically predicted but eludes direct experimental observation is nitrogen (N) vacancies. Here, we unambiguously identify a single N vacancy on a cleaved *m*-plane surface of GaN by direct visualization in real space with scanning tunneling microscopy (STM) and atomic force microscopy (AFM). The presence of a vacancy is established by AFM imaging and force spectroscopy measurements. The identification is accomplished by the analysis of STM images, tunneling current spectroscopy, and comparison with the outcomes from the quantification of band bending near the surface, current calculations, and first-principles simulations. All this information provides insight into the electronic perturbation of a single N vacancy at the surface band structure of GaN. Our results provide further understanding of the effect that point defects have on GaN, and will hopefully contribute to tune the behavior of this technologically relevant material in electronic devices.

DOI: 10.1103/PhysRevB.106.115309

I. INTRODUCTION

Gallium nitride (GaN) is a crucial component in light-emitting diodes, lasers, high electron mobility transistors for wireless communications, and power electronic devices [1–3]. To get the upmost performance from this III-V semiconductor demands the production of high-purity GaN single crystals. The best GaN crystals generally contain a number of atomic defects, which induce localized electronic states in the semiconductor band gap that can largely affect the electronic performance of GaN. Accordingly, point defects in GaN have been intensively studied, both experimentally and theoretically [4–7].

Among various kinds of point defects, single N atomic vacancies are considered to be the most stable native defect [6,8,9] in GaN. It is expected that N vacancies can act as a shallow donor, so that their presence in *p*-type GaN compensate hole carriers [10]. In the latter case, the formation of N vacancy and magnesium acceptor complexes [11] has also been predicted. This charge compensation and the formation of vacancy-magnesium complex are not desirable in devices. In spite of many theoretical studies supporting the existence of N vacancies in GaN, experimental approaches to characterize this defect are scarce. In the case of Ga vacancies and their complexes, they can be measured by positron annihilation [5,12–14], but this technique has a low capability for the detection of the positively charged N vacancies.

*SAGISAKA.Keisuke@nims.go.jp

In terms of spatial resolution, scanning tunneling microscopy (STM) and atomic force microscopy (AFM) have shown advantage to locate individual point defects at surfaces, and probe their morphology and electronic structure. In particular, cross-sectional STM measurements have been pivotal in identifying point defects and dopant atoms in cleaved surfaces of other semiconductors, such as GaAs [15–17] and InP [18–20]. Here, we present the identification of a N vacancy defect at the surface of *n*-type GaN single crystals by using cross-sectional scanning probe microscopy. Atomic resolution AFM was used to corroborate that the structure of this point defect corresponds to an atomic vacancy. The combination of imaging, a thorough analysis of scanning tunneling spectroscopy, and density functional theory (DFT) permitted us to quantify the band bending near the surface, characterize the electronic states of the N vacancy, and successfully simulate the features displayed in the experimental STM images of the defect.

II. METHODS

A. Experiment

The samples were cut from hydride vapor phase epitaxy *c*-plane GaN wafers (*n*-type, Si and O doped, with a typical carrier concentration of 1.45×10^{18} cm^{-3}). The experiments were performed in an ultrahigh vacuum (UHV) low-temperature (LT) STM (Unisoku USM-1200) and a home-built UHV-LT-AFM. The samples were cleaved in UHV prior to the measurements to expose defects in the *m*-plane surface. Both STM and AFM measurements were done using

 ©2022 American Physical Society

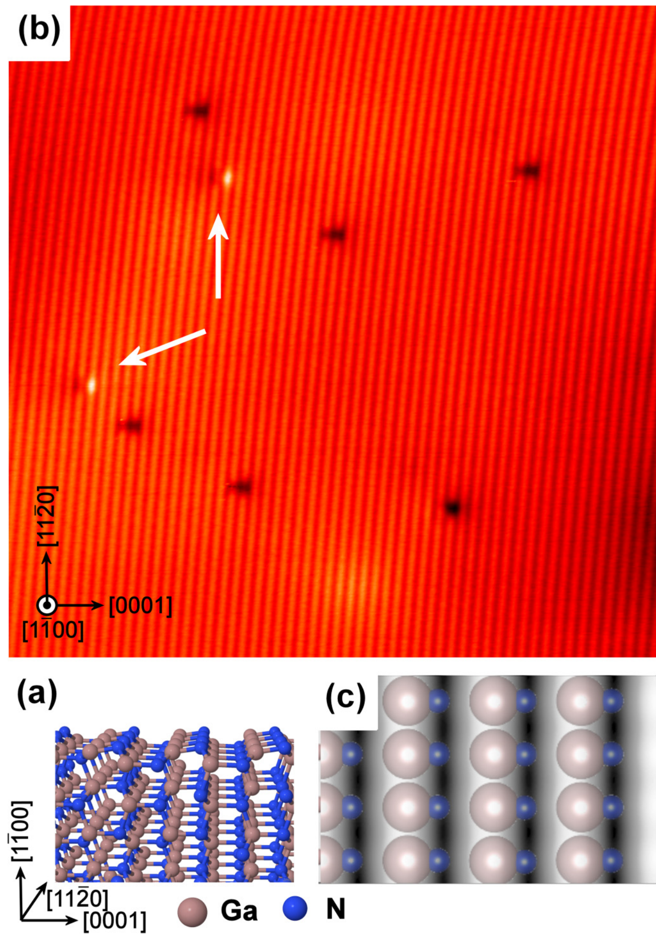

FIG. 1. (a) Ball-and-stick model of a normal *m*-plane surface of GaN. (b) Topographic STM image of a cleaved (1$\bar{1}$00) surface of GaN. Image parameters are size (28.7 × 28.7) nm^2, sample bias voltage (V_s) +2.7 V, current set point (I_t) 10 pA, and temperature (T) 78 K. (c) Simulated STM image of a GaN(1$\bar{1}$00) surface setting $V_s = +2.5$ V. The topmost bilayer of the surface model has been superimposed to the image.

tungsten tips. In our UHV systems (base pressure <5.0 × 10^{-9} Pa), the sample surface was kept in an extremely clean condition: no adsorbates from the residual vacuum were detected in experiments even as long as one month. We usually completed the single characterization of a sample either by STM or by AFM within five days or less after cleavage. The experiments were reproduced several times using a few tens of samples from different locations of the GaN wafer.

B. Computation

STM image simulations were conducted using BSKAN codes [21] under the Tersoff-Hamann approximation [22], which makes use of a set of wave functions generated by DFT calculations performed by the VASP code [23,24]. We employed the projector augmented wave method with a kinetic energy of 500 eV, and the generalized gradient approximation

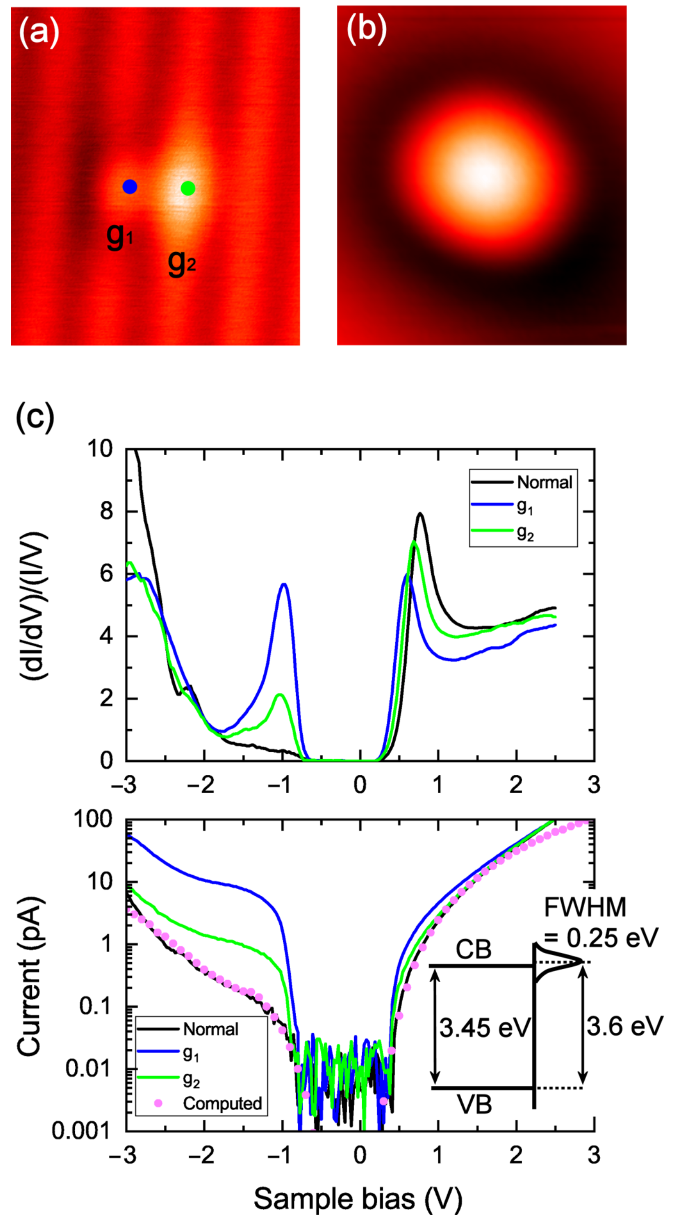

FIG. 2. (a) Unoccupied states ($V_s = +2.5$ V) and (b) occupied states ($V_s = -3.0$ V) STM images of a N vacancy defect at the GaN surface. Additional image acquisition parameters are (28.7 × 28.7) nm^2, $I_t = 10$ pA and $T = 78$ K. (c) Tunnel spectra representing the differential normalized conductance $[(dI/dV)/(I/V)]$ (top) and current (I) (bottom) vs the sample bias (V) recorded over a normal GaN dimer (black), and over the g_1 (blue) and the g_2 (green) sites highlighted with the same color code as in (a). The spectra acquisition set point parameters are $V_s = +2.5$ V, $I_t = 10$ pA, $T = 78$ K. In the lower graph, an $I - V$ curve computed for a normal spot on the GaN surface using SEMITIP [31] is represented by pink dots. The best fit was obtained for a contact potential difference of 0.8 V, a position of the surface state measured from the valence band edge of 3.6 eV and a width of the surface state of 0.25 eV, as sketched in the inset. For the computation, we assumed a density of 6×10^{14} cm^{-2} for the surface state, corresponding to the density of the Ga atom in the surface, and a tip-sample separation of 0.9 nm.

with either the Perdew-Burke-Ernzerhof (PBE) exchange-correlation functional [25] or the Heyd-Scuseria-Ernzerhof (HSE) screened hybrid functional [26]. The GaN($1\bar{1}00$) surface was modeled by a slab consisting of 12 atomic layers. The bottom layer was terminated by pseudo-hydrogen atoms with a fractional charge of 1.25 (0.75) for Ga (N) atoms, and the vacuum space was more than 16 Å thick. The sizes of the surface cell and Monkhorst-Pack k-point grid in the Brillouin zone have a 4×4 and a $2 \times 2 \times 1$ periodicity, respectively. The structural optimizations were performed by PBE until the forces were less than 0.01 eV/Å. The density of states was calculated by the HSE hybrid functional.

III. RESULTS AND DISCUSSION

A. STM imaging of the *m*-plane surface of GaN

The structural model of the nonpolar ($1\bar{1}00$) surface of GaN is shown in Fig. 1(a). In this surface, Ga and N atoms form dimer rows oriented in the [$11\bar{2}0$] crystal direction. Our DFT calculations predict a configuration in which the topmost N atoms protrude 27 pm from the nearest Ga atoms, and the Ga-N dimers sustain a bond length of 183 pm, which agrees with previous works [27–29].

Figure 1(b) shows a STM image of an atomically flat m-plane surface of GaN. The typical terrace size that we obtain after the cleavage of the crystal is a few-hundred-nanometers wide. The stripes observed in the image correspond to the Ga-N dimer rows. A simulated STM image for a sample bias of +2.5 V [Fig. 1(c)] allows us to assign these stripes to unoccupied dangling bond states extending predominantly over the Ga site of the dimers, in agreement with previous reports [27–30]. Besides the features associated with the Ga-N dimer rows, the STM image in Fig. 1(b) displays several defects: two bright features pointed by white arrows, and six hollow features. In this work, we focus our efforts on clarifying the nature of these bright defects, which we have identified as single N vacancies.

Figure 2 shows detailed STM images of one of the defects pointed by an arrow in Fig. 1(b), together with tunnel spectra acquired over it. The density of this type of defect at the surface of the sample is 8.0×10^{10} cm^{-2}. For positive sample bias voltages, this defect presents two bright features with different sizes, labeled as g_1 and g_2 in Fig. 2(a). Tunnel spectra in the form of the normalized differential conductance (dI/dV) recorded over g_1 and g_2 [upper panel of Fig. 2(c)] show peaks at slightly lower sample bias voltage than the peak observed at +0.8 V, which was measured over a normal GaN dimer (black curve). The latter corresponds to an unoccupied dangling bond state extending over the Ga atoms.

For negative sample bias voltages, the same defect is imaged as a bright round protrusion spatially extending over the width of two GaN dimer rows [Fig. 2(b)]. Such a bright feature originates from the electronic state at −1.0 V in the spectra of Fig. 2(c) and its additional electrostatic effect around the point defect. In imaging with a negative sample bias voltage, normal GaN dimers do not appear as rows in the STM image, in contrast to imaging with a positive sample bias voltage. The dark ring [Fig. 2(b)] or oscillation behavior [Fig. 7(b) in the Appendix] surrounding the bright feature is reminiscent of a charged defect in a semiconductor [32,33]. The spectrum recorded at a normal GaN dimer far from the defect (black curve) does not present any peaks at negative bias voltages: instead, it shows an onset at −0.9 V, followed by a broad feature up to −2.0 V, and an abrupt increase in the conductance up to −3.0 V. Therefore, when exploring the surface with negative bias voltages, instead of imaging the dangling bond state over the N atoms of the dimers, we probe the bottom of the s-orbital-like conduction band state around the Γ point [27,30] and the tunnel current is supplied by carriers in the conduction band owing to a heavy n-type doping, as sketched in Fig. 6(c). Accordingly, the bright protrusion with the dark ring surrounding the defect in Fig. 2(b) should be caused by a screening effect of the conduction band carriers, which suggests that this defect is positively charged.

To gain further insight into the tunneling process in STM experiments on this surface, we have fitted a tunnel current spectrum acquired over a normal GaN spot using the program (SEMITIP, ver. 5) developed by Feenstra [31,34–36], that allows computation of the electrostatic potential in a semiconductor surface under the presence of a metallic probe tip and corresponding tunnel current between them. In this simulation, an acceptorlike surface state modeling the dangling bonds of the surface Ga atoms was incorporated in the calculation of the electrostatic potential distribution. The fit is plotted as a dotted curve over the experimental counterpart; see the lower panel of Fig. 2(c). The best fit is obtained when assuming (i) a surface state with a Gaussian shape of 0.25 eV full width at half maximum, located 3.6 eV above the valence band edge, and (ii) a contact potential difference between the probe and surface of 0.8 eV. In spite of being a heavily n-type doped sample, whose Fermi level (E_F) should be located above the conduction band edge [37], the onset of the current for the positive sample bias occurs at ∼0.4 V, as shown by the current spectra in the lower panel of Fig. 2(c). This shift in the voltage value for the current onset is due to the contact potential difference between probe and surface. We have quantified the band bending due to this contact potential difference (Fig. 11) and, for $V_S = 0$ V, the bands near the surface are shifted towards positive values by 0.33 eV, and for $V_S = +0.4$ V (which is the bias voltage for the current onset), the bands are shifted by 0.53 eV (arrows in Fig. 11).

The current emerging in the range of −0.9 to −3.0 V is attributed to tunneling of electrons from the bottom of the conduction band. The band bending reaches a flat condition at $V_S = -0.9$ V (see Fig. 11). Applying higher negative sample bias causes the bands to bend downwards near the surface. Because of tunneling from the accumulation region, the size of the apparent band gap observed in our experiments [approximately 1.3 eV; see Fig. 2(c)] appears smaller than the typical band gap of GaN (∼3.45 eV [38,39]). Furthermore, the experimental evidence that the quantity of tunnel current for negative sample biases is considerably smaller than that for positive ones is characteristic of a pinning effect of the bands near the surface: surface charges arising from the occupation of the surface state restrict further tip-induced band bending, thus leading to the tunnel current from the accumulation layer being suppressed [36]. Fitting attempts by positioning the surface state at other energies did not provide an acceptable agreement, giving rise to the inception of the pinning effect

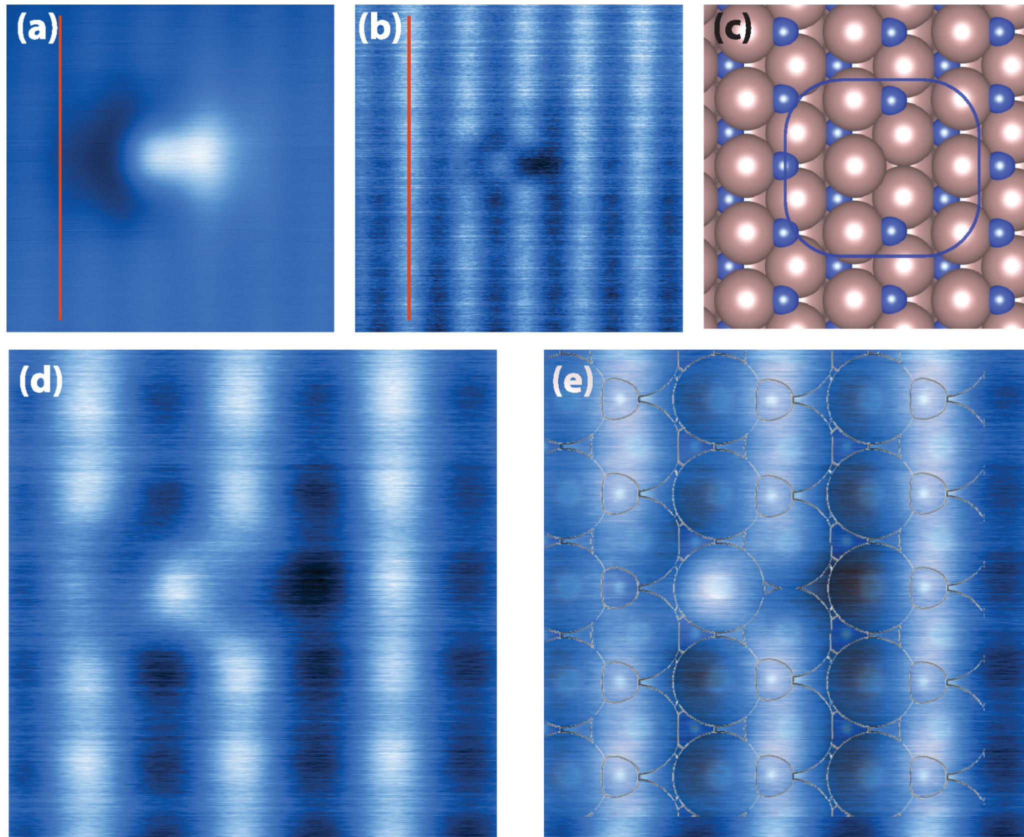

FIG. 3. Constant height (a) STM and (b) AFM images of a N vacancy. (c) Model of a N vacancy in the surface produced from our first-principles calculations. (d) High-resolution constant height AFM image of the defect obtained by approaching the probe 50 pm towards the surface with respect to the image in (b). (e) Superposition of the model in (c) to the image in (d) for the identification of the atomic species imaged with the AFM (see text for details). Image size and bright-dim look-up-table limits are (3 × 3) nm^2, (143.4, 32.8) pA and (−0.9731, −1.8526) Hz for (a) and (b), respectively; (3 × 3) nm^2 and (−1.208, −1.611) Hz for (d) and (e). Free-oscillation resonant frequency and oscillation amplitude were 999 746 Hz and 40 pm, respectively.

at inappropriate sample bias voltages either in the case of a surface state placed fully inside the band gap or placed fully in the conduction band. The complete absence of a surface state induces a larger band bending towards lower energies and the formation of quantized (localized) states in the accumulation region [Fig. 12(b)]. Additionally, the current from the valence band emerges for $V_S < -3.5$ V, but its contribution to the total current is negligible compared to that of the conduction band [Fig. 12(a)]. A similar computational analysis was done by Schnedler *et al.* [40], in which a surface state was set within the band gap to explain the band bending required to shift the onset voltage for a positive sample bias, but this model failed to explain tunneling from the accumulation region with a negative sample bias. Our model can, however, comprehensively explain the tunneling process on the GaN surface for both positive and negative biases.

B. AFM imaging of the *m*-plane surface of GaN

The type of defect described in Fig. 2 was also characterized by atomic force microscopy (AFM) operated in noncontact mode [41–43] using constant oscillation amplitude. This technique, at variance with the STM, is less dependent on the electronic nature of the surface and relies more on the atomic structure [44,45], as the signal that produces atomic contrast is due to the onset of a chemical bond formation between the outermost atom of the probe and the atoms at the surface [46,47].

Figures 3 and 4 summarize a series of imaging and force spectroscopy measurements carried out over a defect found at the *m*-plane surface of GaN that exhibited a similar STM signal as the one displayed in Fig. 2(a). Since the AFM experiments reported here were performed using the KolirbiSensor [48], it is possible to detect both STM and AFM signals over the same surface spot.

Figure 3(a) shows the tunnel current registered over the defect by scanning at a constant height with a sample bias voltage of +2.5 V. This signal closely resembles the topographic STM image presented in Fig. 2(a), with two current maxima—one more extended than the other—placed at adjacent dimer rows, and a current depletion close to the less extended current maximum. An AFM image measured exactly at the same surface spot is displayed in Fig. 3(b). This image was acquired with a bias voltage of +1 mV to prevent any possible interference of the tunnel current in the force detection (at this bias voltage, only background noise is detected in the STM signal). The AFM image presents a quite different appearance than the STM one: bright stripes of atomic rows are clearly distinguished. The position of these atomic rows lies in between the stripes of high current in

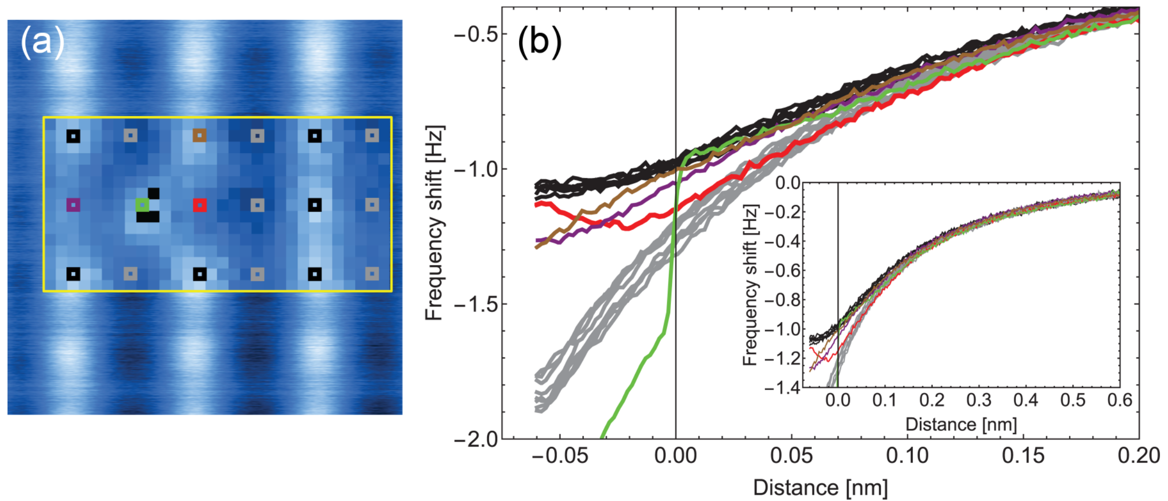

FIG. 4. (a) AFM image extracted from a force volume measured over the area surrounding the N vacancy and enclosed by a yellow square, superimposed to the image shown in Fig. 3(d). (b) Graphs with representative curves exacted from the force volume. The color code of the curves matches the colored pixels in (a). The inset depicts the same curves over the whole probe-surface separation explored. The origin in the horizontal axis corresponds to the separation as for the acquisition of the inset image in (a). Image size and bright-dim look-up-table limits for the enclosed image are (1.5×0.75) nm^2 and $(-1.119, -1.762)$ Hz. Free-oscillation resonant frequency and oscillation amplitude were 999 746 Hz and 40 pm.

the STM image, as it is highlighted by the line in Figs. 3(a) and 3(b), which marks the same position in both images. An even more striking difference is the appearance of the AFM signal at the defect location: a shift of the bright contrast in the AFM signal to one side of the atomic row is clearly detected. To understand the information provided by the AFM in this region, we need to identify the atomic species imaged by the AFM and study the local variation of the force field around the defect.

Aiming at correlating the maxima in the AFM signal in Fig. 3(b) with the atomic species of the *m*-plane surface of GaN, we have compared a high-resolution AFM image of the defect [Fig. 3(d)] with the calculated atomic structure of a N vacancy [Fig. 3(c)]. To make a suitable correspondence, the STM image shown in Fig. 3(a) was scaled and aligned with an image formed by the simulated STM image for a bias voltage of +2.3 V and a E_F positioned at −0.5 eV displayed in Fig. 5(b) with the corresponding calculated atomic lattice superimposed to it. The model with the vacancy depicted in Fig. 3(c) was then scaled and aligned with the atomic lattice over the calculated STM signal, and the three images were then superimposed to the AFM image shown in Fig. 3(b). Scaling and aligning the high-resolution AFM image presented in Fig. 3(d) to the latter provided a hint to ascribe the location of the bright contrast in the AFM signal [49]. This process resulted in the composed image shown in Fig. 3(e). At the probe-surface separation range at which the AFM images in Fig. 3 were acquired, the bright spots in the AFM signal lie over the N atoms of the surface, while the atomic positions ascribed to Ga atoms in the normal surface present a lower AFM signal.

In contrast to the case of the STM, the signal sensed with an AFM is not a monotonic function with the probe-surface separation: depending on the relative interaction of different atomic species at a surface with the outermost atom of the probe, and the distance at which they are sensed, the image contrast can vary—and even invert [50]—from one atomic position to another. To clarify the force range at which AFM images are acquired, it is crucial to perform force spectroscopy measurements at each of the surface positions of interest. To this end, we have measured a force volume [51] over the region surrounding the defect: a (1.5×0.75) nm^2 area above the defect was divided in (30×15) pixels, and a force curve [46,52] of 512 points was acquired at each pixel. The force volume provides then a total of 450 force curves mapping the region surrounding the defect or, alternatively, 512 images characterizing the local variation of the probe-surface interaction over the separation explored in the force curves. Enclosed by a yellow square in Fig. 4(a), an image from the force volume is displayed superimposed to the high-resolution AFM image depicted in Fig. 3(d). The enclosed image corresponds to the AFM signal at the origin of displacement in the force curves, which is just 10 pm closer to the surface than the probe-surface separation at which the AFM image in Fig. 3(d) was acquired. The image shows the (30×15) pixelation characteristic of the force volume acquisition. A representative selection of force curves extracted from the force volume is displayed in Fig. 4(b).

The force curves registered over the locations ascribed to the N and the Ga atoms far from the defect are colored as black and gray, respectively, and the pixels at which these curves were acquired are highlighted by squares of the same color in Fig. 4(a). Upon inspecting these curves, we can assert that both bright and dim contrast in the AFM images of Fig. 3 reflect an attractive interaction force between the surface atoms and the outermost atom of the probe, and that contrast inversion does not occur. The groups of force curves measured over the N and the Ga atoms far from the defect exhibit almost identical behavior, respectively. Over the N atoms, the AFM signal is close to reach its minimum, while at the Ga atoms,

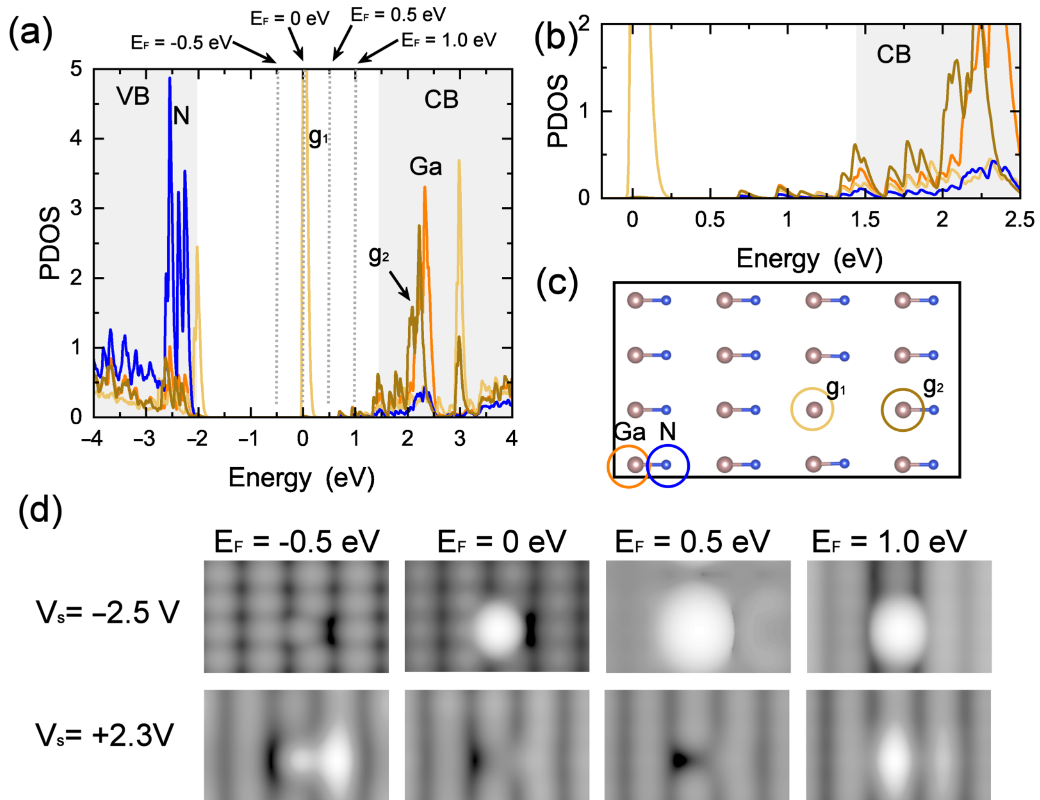

FIG. 5. (a) Projected density of states (PDOS) for a Ga-N dimer and a N vacancy. The energy origin corresponds to E_F, which is determined by the electron occupancy. Gray regions denote the bulk valence band (VB) and conduction band (CB) obtained from the PDOS for Ga and N atoms in the middle of the slab. (b) Zoom-in plot of the region around the CB edge. (c) The 4×4 surface cell used for calculations. (d) Simulated STM images of a N vacancy for various positions of E_F. STM images were generated with an isosurface value of 1.0×10^{-6} e/Å^3.

the interaction is still monotonically decreasing. The presence of a minimum in the AFM signal is characteristic of the onset of a bond formation between probe and surface atoms, and a monotonic decrease indicates either that the AFM signal is still dominated by a long-range force or that the interaction between the closest probe and surface atoms is still strongly attractive at the explored separation range. This behavior of the force curves confirms that the bright spots at the pristine areas of the AFM images in Fig. 3 correspond to imaging the topmost layer of the surface (the N atoms protrude 27 pm above the Ga atoms in the dimers), and confirms that the AFM is sensitive to the atomic arrangement—rather than to the electronic structure—of this surface.

The force curves measured at locations close to the defect display a different behavior. The curve measured at the spot of the missing N atom (red curve and square, respectively) presents a minimum in the AFM signal, which is more attractive and slightly shifted to larger probe-surface separations than the ones exhibited by the N atoms of the pristine surface. The force curves over the Ga atom with a dangling bond exhibit quite an unstable behavior (green curve and square): upon approaching the probe towards the surface, the AFM signal suddenly jumps to more attractive values. This is the origin of the pixels with a black contrast in the enclosed image of Fig. 4(a), which bear the most attractive values of the AFM signal in the image. Such behavior is characteristic of the transition between different energy solutions of the probe-surface interaction due to the jump of a surface atom towards the AFM probe [53]. Since the probe shows a stable behavior over the rest of the explored surface area, the instabilities in the AFM signal are characteristic of the atom probed at this surface location. This unstable behavior of the Ga atom with a dangling bond may also be responsible for the slightly different behavior of the force curves measured over the N atom positions at the left (purple curve and square) and upper part (brown curve and square) of the defect.

The AFM images and the force spectroscopy measurements support the hypothesis of a N vacancy as the origin of the defects displayed in Figs. 2 and 3. The instabilities exhibited by the Ga atom left with a dangling bond are a clear indication of a N atom missing. The lack of coordination makes this Ga atom protrude 31 pm with respect to the Ga atom layer of the normal surface. This makes the Ga atom able to be seen by the AFM almost at the same height as the N atoms. The red curve at the position of the vacancy is also an indication of the absence of a N atom. The drop of the AFM signal towards the minimum resembles the behavior of the signal detected over the Ga atoms, rather than the one over the N atoms. The presence of a minimum in the curve is probably due to the interaction of the probe outermost atom with the Ga atom with a dangling bond and with the adjacent N atoms of the same row, which relax 9 pm towards the empty space created by the vacancy.

C. STM simulation for nitrogen vacancy

To understand the STM image contrast in our experiments, we carried out first-principles calculations under the DFT framework. Simulating our experimental STM images requires one to first characterize the electronic structure of the area surrounding the N vacancy. Figure 5(a) shows the projected density of states (PDOS) for a Ga-N dimer, a Ga atom next to the N vacancy (g_1), and a Ga atom of the dimer adjacent to the vacancy (g_2) [see Fig. 5(c)]. The calculated bulk band gap is 3.46 eV, which is similar to the typical value (3.45 eV [38,39]). The influence of the N vacancy is localized within the Ga-N dimer row containing the vacancy and the adjacent row, so that the PDOS for the Ga-N dimer shown in Fig. 5(a) approximates the electronic features far from the vacancy.

Occupied and unoccupied surface states are mainly distributed over the N and the Ga atoms, respectively. The majority of the unoccupied surface states overlap at the conduction band, but they extend by ~ 0.8 eV into the band gap below the conduction band edge [Fig. 5(b)], in agreement with previous works [27,30]. This panorama qualitatively tallies with the assumption of the unoccupied surface state penetrating by ~ 0.1 eV into the band gap used to fit the tunnel current spectrum in Fig. 2(c). This smaller penetration value with respect to the one obtained from the DFT is probably due to the surface state being represented by a simple Gaussian function in our fitting model.

The characteristic electronic state of the N vacancy at the surface is found over the g_1 atom, 2.2 eV above the valence band edge ($\sim$1.2 eV below the conduction band edge). This energy state contrasts with the one of a bulk N vacancy, reported to be $\sim$44–64 meV below the conduction band edge [10,54,55]. According to this relatively large energy value to reach the conduction band, a N vacancy at the top surface will not act as a dopant. The absence of the N atom also slightly affects the electronic structure of the Ga atom of the closest dimer (g_2), which shows a similar peak to a normal Ga atom but slightly shifted towards a lower energy and with a tail falling into the surface band gap.

The simulation of the experimental STM images also requires a well-defined position of the Fermi level. However, the influence of the doping (n-type or p-type semiconductor) and the band bending induced by the electric field of the STM tip—factors that affect the position of the Fermi level in the experiments—is not taken into account in our DFT calculations due to the finite size of the slab. This limitation can be overcome by comparing sets of calculated STM images for several bias voltages and positions of the Fermi level with the experimental counterparts. Figure 5(b) shows STM images of a N vacancy at the m-plane surface of GaN, which were simulated based on wave functions produced by a hybrid exchange-correlation functional [26]. These STM images were obtained by integrating the electronic states over the range between the Fermi level and the energy associated to the sample bias voltage displayed in the figure (eV_S). For an E_F set to 0 eV, as determined by the electron occupation for the neutral slab, given in Fig. 5(a), the STM image for $V_S = +2.3$ V does not show the characteristic bright features observed in the experiments; see Fig. 2(a). The image for

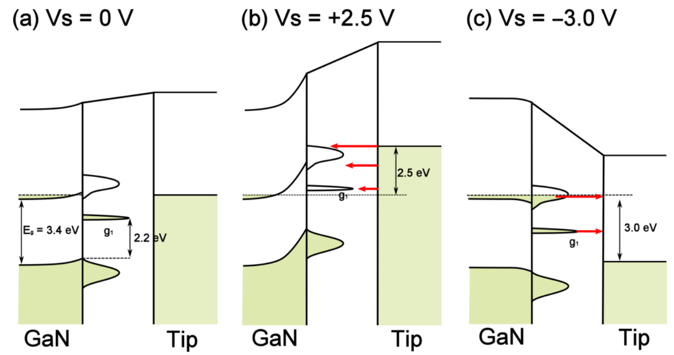

FIG. 6. Diagram for tunneling processes between the STM tip and the m-plane surface of n-type GaN in the vicinity of a N vacancy: (a) equilibrium, (b) unoccupied state imaging, and (c) occupied state imaging. g_1 corresponds to the state observed in Fig. 5(a).

$V_S = -2.5$ V reproduces the bright features, but their spatial extension is smaller than the one observed in the experimental ones; see Fig. 2(b). For an E_F set to -0.5 eV, as to integrate the electronic state of g_1 into an unoccupied state image ($V_S = +2.3$ V), the characteristic features of the N vacancy in Fig. 2(b) are perfectly reproduced. Similarly, a STM image displaying a spatially extended bright feature close to the one in the experiments is reproduced for an E_F set to $+0.5$ eV, as to integrate the state of g_1 into the occupied state image ($V_S = -2.5$ V). Setting an E_F to $+1.0$ eV, so that the bottom of the unoccupied Ga state contributes to the STM image, produces STM images where a bright feature over the vacancy together with the features ascribed to the rows of Ga atoms in the experiments appear at a negative voltages (-2.5 V). However, the latter is not observed in the experiments. In addition, the features displayed in the experimental STM images are not reproduced when carrying out this analysis for a single Ga vacancy (see Fig. 8). These results allow us to conclude that the defect observed in Figs. 2(a) and 2(b) is certainly assigned to a single N vacancy. Furthermore, we demonstrated that the appropriate tuning of the Fermi level in the simulations is fundamental to reproduce the experimental images of a semiconductor surface.

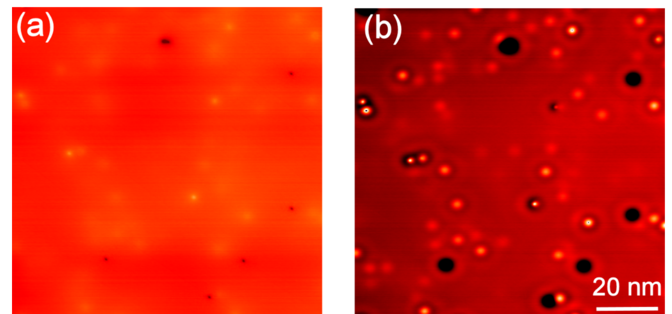

FIG. 7. Topographic STM images of the same area of the m-plane GaN surface measured at 78 K with a current set point of $I_t = 10$ pA. The acquisition parameters were (a) $V_S = +0.3$ V, (b) $V_S = -0.3$ V. Image size is 100×100 nm.

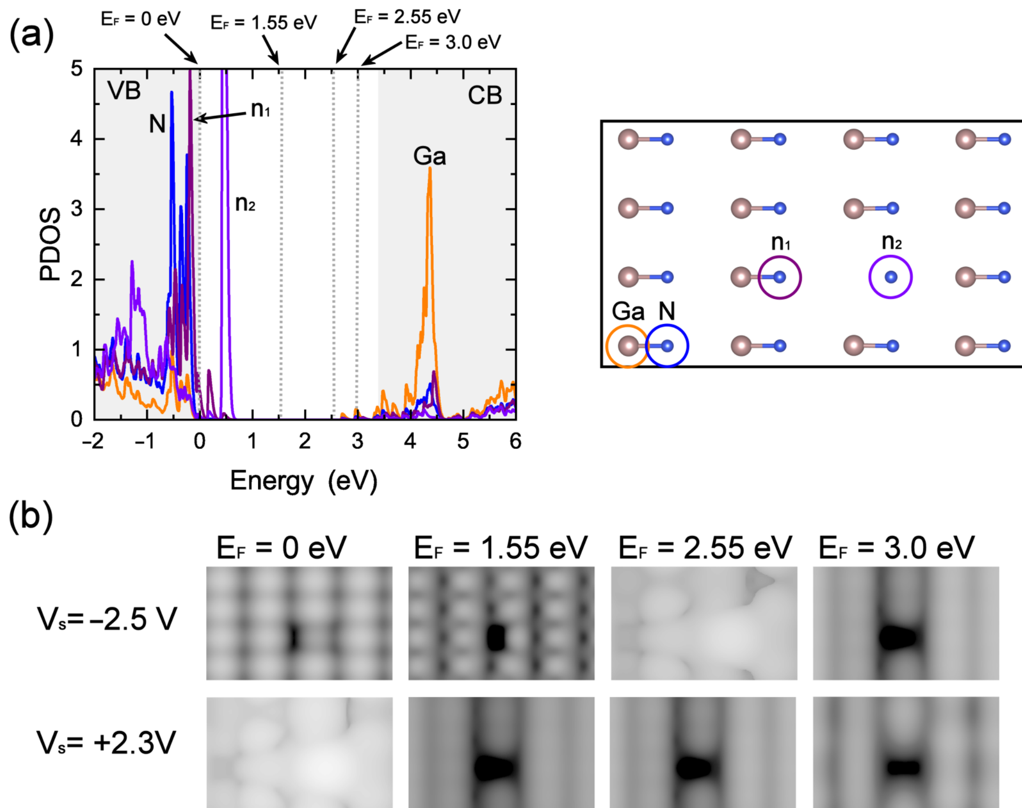

FIG. 8. PDOS and STM images simulated for a Ga vacancy. Gray regions denote the bulk valence band (VB) and conduction band (CB) obtained from the PDOS for Ga and N atoms in the middle of the slab. STM images were generated with an isosurface value of 1.0×10^{-6} e/Å^3.

D. Nitrogen vacancy state in the surface

The combination of the calculated electronic states and fitting of the experimental tunneling spectroscopy curves allows us to shed light on the electronic state of the surface N vacancy and the tunneling processes between the probe and the surface. From the experiments, the electronic state of the N vacancy appears at −1 V [Fig. 2(c)], whereas our DFT calculations position the electronic state of the vacancy 2.2 eV above the valence band edge [Fig. 5(a)]. Since the contribution of the valence band to the current in the experiments is much smaller than the contribution of the conduction band for large negative bias voltages [Fig. 12(a)], it is difficult to distinguish the edge of the valence band from the tunneling spectra and subsequently to determine the energy position of the N vacancy from the valence band edge experimentally. However, provided that the same amount of band bending occurs at the surface independently of being at a normal or a defective site, our computational results of band bending allow us to estimate that the state of the N vacancy appears at a sample bias of −1.28 V, which agrees well with the experimental observation around −1.0 V. The slight deviation in the energy may be caused by local charges at the N vacancy. Upon these observations, we can put forward a band diagram for the tunneling processes between the STM tip and the *n*-GaN surface (Fig. 6). Since the sample used in this study was a heavily doped *n*-type semiconductor, the Fermi level should be located near the conduction band edge. Both the results of the calculations of tunneling current in Fig. 2(c) and the PDOS in Fig. 5 show that an unoccupied Ga state is located within the bulk conduction band, but its tail penetrates into the bulk band gap. The state of the N vacancy (g_1) in the surface is located at 2.2 eV above the valence band edge, which contributes to both unoccupied [Fig. 6(b)] and occupied [Fig. 6(c)] state imaging through a tip-induced band bending. When a positive sample bias is applied (V_S ∼ +2.5 V), the conduction band near the surface is bent upwards. As a result, a current onset is observed around 0.5 V over a normal site and at a smaller bias over the N vacancy site [Fig. 2(c)]. On the other hand, when a negative sample bias is applied, the current from the conduction band starts flowing around $V_S = -0.9$ V [Fig. 2(c)] and, simultaneously, a pinning of the band occurs by the presence of the surface state. Over a wide range of the negative sample bias, at least down to −6.0 V [Fig. 12(a)], the current is dominated by the contribution from the conduction band. Particularly, a large current is obtained from the N vacancy site around −1.0 V, resulting in imaging of the bright feature over it. Our interpretation of the tunnel process differs from that of Schnedler *et al.* [40]: they assume that the entire surface state is located inside the band gap and, as a result, pinning of the bands occurs only at small positive voltages but not at negative voltages. In contrast, our results show that to comprehensively reproduce the tunnel process on the *m*-plane surface of GaN, the surface state has to be located at the conduction band with its tail penetrating into the band gap.

IV. CONCLUSION

In conclusion, we demonstrate the imaging of a single N vacancy in the *m*-plane surface of a cleaved GaN crystal by STM and AFM. We observe a single atom vacancy in the row of Ga-N dimers, which was determined by the analysis of combined imaging and force spectroscopy measurements with AFM. This defect is identified as a N vacancy by the comparison of experimental STM images with those simulated for a N vacancy and a Ga vacancy. These STM images were calculated by systematically tuning the Fermi energy to account for the crystal doping and the tip-induced band bending. A theoretical fitting to the experimental tunnel current provides insight into the electrostatic potential in the surface of GaN upon the interaction with the electric field of the STM tip. The electronic state of the N vacancy in the surface was found at 2.2 eV above the valence band edge. This represents an experimental demonstration of the presence of a N vacancy in GaN.

ACKNOWLEDGMENTS

This work was supported by the MEXT Program for the research and development of next-generation semiconductors to realize an energy-saving society. The calculations in this study were performed on the Numerical Materials Simulator at NIMS.

APPENDIX A: WIDE-AREA STM IMAGE OF THE *m*-PLANE SURFACE OF GaN

Figure 7 shows STM images of the same region of the *m*-plane surface of GaN. For positive sample bias voltages, shown in Fig. 7(a), several surface defects showing bright and dark features are observed. The image for negative bias voltages, shown in Fig. 7(b), presents a wide variety of features (some of them surrounded by a ring) associated to surface defects and to dopants at different depths. Similar features have been reported for the GaAs (110) surface [32].

APPENDIX B: SIMULATED STM IMAGES FOR A Ga VACANCY AND OTHER IMPURITIES IN THE *m*-PLANE SURFACE OF GaN

Figure 8 shows the calculated projected density of states (PDOS) of a Ga vacancy, together with two sets of STM images simulated for various values of E_F. The electronic states at n_1 and n_2 are situated near the occupied surface state of N. These simulated STM images do not reproduce any of the features experimentally observed in Fig. 2.

According to the analysis of the force spectroscopic data in Fig. 4, the point defect discussed in the main text has been ascribed to an atomic vacancy. Here, to reinforce the identification of the defect as a N vacancy, we present simulations of the electronic states and corresponding STM images for other possible atomic impurities such as an Si atom at a surface Ga site, an O atom and a C atom at a surface N site. At variance with the calculations presented in the main text, the simulations for these impurities were carried out using the less computationally costly PBE functional. To confirm the validity of this functional, we first compared the results of the PDOS and simulated STM images for a N vacancy calculated using PBE (Fig. 9) and HSE06 (Fig. 5). Although the PBE underestimates the band gap (2.06 eV against 3.46 eV obtained with HSE06), the general features in the electronic state of the Ga-N dimer as well as the N vacancy induced states provided by this functional are very similar to the ones obtained with HSE06. Furthermore, the simulated STM image for the N vacancy obtained with PBE nicely reproduces the experimental features in both occupied and unoccupied state images. Thus, PBE is a reasonable selection to support the interpretation of the STM images in Fig. 2.

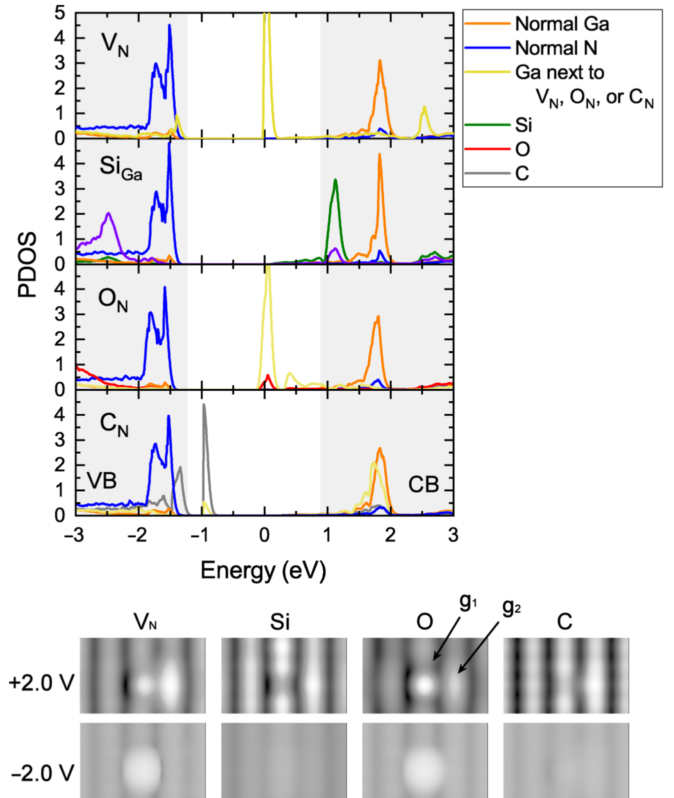

FIG. 9. PDOS and STM images simulated for the cases of an Si atom placed at a Ga site (Si_{Ga}), an O atom at a N site (O_N), and a C atom at a N site (C_N), in comparison with those of a N vacancy (V_N). At variance with the simulation shown in the main text, for these calculations we used the PBE functional instead of the more computationally costly HSE06 functional. Gray regions denote VB and CB. For the STM image simulations, the Fermi level was set at +0.5 eV for occupied state images and −0.5 eV for unoccupied state images. STM images were generated with an isosurface value of 1.0×10^{-6} e/Å^3.

Figure 9 shows that an O atom induces a similar state to the N vacancy at the Fermi level, while Si and C atoms induce new states at different energies. As a result, the simulated STM images for the O atom at the surface resemble those for the N vacancy. However, the image contrast at the g_1 and g_2 sites differs between the N vacancy and O atom. The N vacancy still gives the best agreement with the experimental image in Fig. 2.

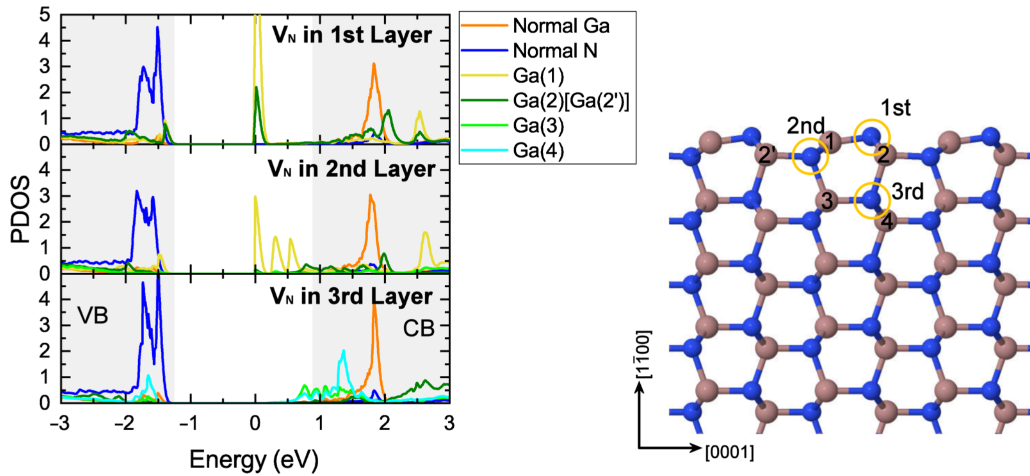

FIG. 10. PDOS for Ga atoms surrounding a N vacancy placed at the first, second, or third atomic layer of the surface. The electronic convergence was performed using PBE. Numbering of the Ga atoms at the plot correlates with the numbering at the stick-and-ball model. Gray regions denote VB and CB.

APPENDIX C: DEPTH DEPENDENCE OF THE N VACANCY STATE

We have shown that an electronic state induced by a surface N vacancy appears 1.2 eV below the conduction band edge (Fig. 5), which differs from the situation of a N vacancy in the bulk. Figure 10 shows a transition of the electronic state of the N vacancy upon deepening its position towards the bulk. For this calculation, we used the PBE functional, which underestimates the size of the band gap of GaN, as mentioned above. Nevertheless, this result shows that the N vacancy induced state, which locates in the band gap when the N vacancy is at the topmost surface, tends to approach the conduction band edge as the position of the N vacancy deepens towards the bulk.

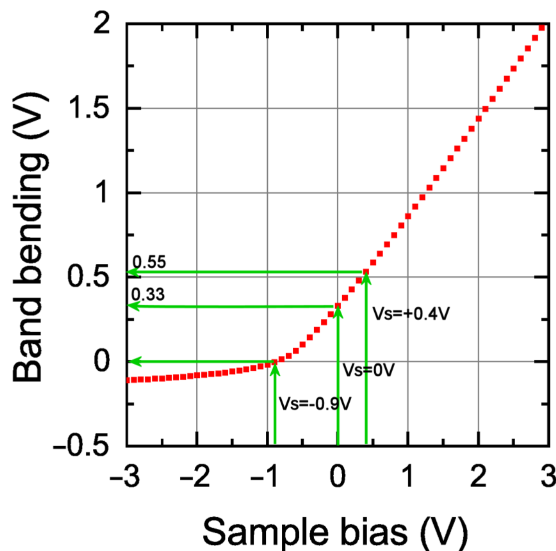

FIG. 11. Band bending in the GaN surface as a function of sample bias calculated for the configuration displayed in the inset of Fig. 2(c).

APPENDIX D: ADDITIONAL COMPUTATION OF THE TUNNEL CURRENT

Figure 11 presents the band bending calculated as a function of the sample bias (V_S) obtained with the values that

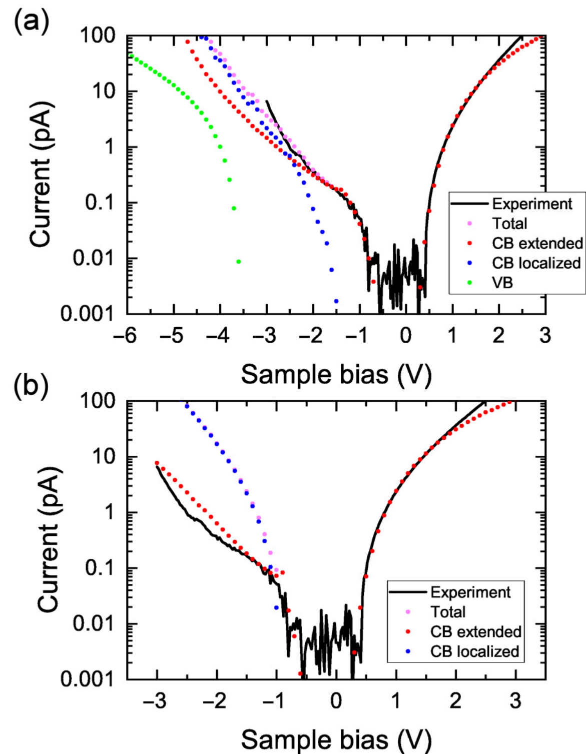

FIG. 12. Calculated component of the tunnel current for a pristine GaN surface (a) considering the surface state and (b) without the surface state. The curves labeled as CB extended and CB localized correspond to the current component derived from the carriers accumulated at the bottom of the bulk conduction band and at quantized states in the conduction band bent downwards, respectively.

provide the best fitting for the tunnel current displayed in Fig. 2(c). For an *n*-type GaN, the surface potential is bent upwards by approximately 0.33 eV when $V_S = 0$ V. By applying a positive sample bias, a large band bending is induced, whereas the application of a negative sample bias lower than -0.9 V hardly changes the surface potential, owing to a pinning effect by the surface state.

By using the parameters obtained from the fitting to the tunnel current spectrum shown in Fig. 2(c), we calculated the contribution of the valence band to the tunnel current down to a sample bias of -6.0 V; see Fig. 12(a). The current arising from the valence band appears at a sample bias voltage of ~ -3.6 V. Even though a large negative sample bias is applied (in a situation where the Fermi level of the tip is fully located in the valence band of the GaN), the tunnel current is mainly dominated by the contribution from the conduction band. Because of the wide band gap of GaN, electrons in the valence band are subject to a larger tunnel barrier than those in the conduction band. A similar result has been reported elsewhere [56].

We also calculated the tunnel current in the absence of the surface state; see Fig. 12(b). Without the surface state, we found that the contribution of the localized state in the conduction band, i.e., the quantized state in the accumulation layer, increases and the total current deviates from the experimental result. Accordingly, the role of the surface state is to pin the potential near the surface against the electric field originated by the presence of the STM tip.

[1] S. J. Pearton, J. C. Zolper, R. J. Shul, and F. Ren, GaN: Processing, defects, and devices, J. Appl. Phys. **86**, 1 (1999).

[2] R. S. Pengelly, S. M. Wood, J. W. Milligan, S. T. Sheppard, and W. L. Pribble, A review of GaN on SiC high electron-mobility power transistors and MMICs, IEEE Trans. Microwave Theory Tech. **60**, 1764 (2012).

[3] I. C. Kizilyalli, A. P. Edwards, H. Nie, D. Disney, and D. Bour, High voltage vertical GaN $p-n$ diodes with avalanche capability, IEEE Trans. Electron Devices **60**, 3067 (2013).

[4] M. A. Reshchikov and H. Morkoç, Luminescence properties of defects in GaN, J. Appl. Phys. **97**, 061301 (2005).

[5] F. Tuomisto and I. Makkonen, Defect identification in semiconductors with positron annihilation: Experiment and theory, Rev. Mod. Phys. **85**, 1583 (2013).

[6] J. L. Lyons and C. G. Van de Walle, Computationally predicted energies and properties of defects in GaN, npj Comput. Mater. **3**, 12 (2017).

[7] M. A. Reshchikov, Measurement and analysis of photoluminescence in GaN, J. Appl. Phys. **129**, 121101 (2021).

[8] M. G. Ganchenkova and R. M. Nieminen, Nitrogen Vacancies as Major Point Defects in Gallium Nitride, Phys. Rev. Lett. **96**, 196402 (2006).

[9] G. Miceli and A. Pasquarello, Self-compensation due to point defects in Mg-doped GaN, Phys. Rev. B **93**, 165207 (2016).

[10] J. Buckeridge, C. R. A. Catlow, D. O. Scanlon, T. W. Keal, P. Sherwood, M. Miskufova, A. Walsh, S. M. Woodley, and A. A. Sokol, Determination of the Nitrogen Vacancy as a Shallow Compensating Center in GaN Doped with Divalent Metals, Phys. Rev. Lett. **114**, 016405 (2015).

[11] U. Kaufmann, P. Schlotter, H. Obloh, K. Köhler, and M. Maier, Hole conductivity and compensation in epitaxial GaN:Mg layers, Phys. Rev. B **62**, 10867 (2000).

[12] K. Saarinen, T. Laine, S. Kuisma, J. Nissila, P. Hautojarvi, L. Dobrzynski, J. Baranowski, K. Pakula, R. Stepniewski, M. Wojdak, A. Wysmolek, T. Suski, M. Eszczynski, I. Grzegory, and S. Porowski, Observation of Native Ga Vacancies in GaN by Positron Annihilation, Phys. Rev. Lett. **79**, 3030 (1997).

[13] A. Uedono, S. Ishibashi, T. Ohdaira, and R. Suzuki, Point defects in group-III nitride semiconductors studied by positron annihilation, J. Cryst. Growth **311**, 3075 (2009).

[14] A. Uedono, S. Ishibashi, K. Tenjinbayashi, T. Tsutsui, K. Nakahara, D. Takamizu, and S. F. Chichibu, Defect characterization in Mg-doped GaN studied using a monoenergetic positron beam, J. Appl. Phys. **111**, 014508 (2012).

[15] C. Domke, P. Ebert, M. Heinrich, and K. Urban, Microscopic identification of the compensation mechanisms in Si-doped GaAs, Phys. Rev. B **54**, 10288 (1996).

[16] J. Gebauer, R. Krause-Rehberg, C. Domke, P. Ebert, K. Urban, and T. E. M. Staab, Direct identification of as vacancies in GaAs using positron annihilation calibrated by scanning tunneling microscopy, Phys. Rev. B **63**, 045203, (2001).

[17] D. Tjeertes, T. J. F. Verstijnen, A. Gonzalo, J. M. Ulloa, M. S. Sharma, M. Felici, A. Polimeni, F. Biccari, M. Gurioli, G. Pettinari, C. Sahin, M. E. Flatte, and P. M. Koenraad, N-nH complexes in GaAs studied at the atomic scale by cross-sectional scanning tunneling microscopy, Phys. Rev. B **102**, 125304 (2020).

[18] P. Ebert, M. Heinrich, M. Simon, C. Domke, K. Urban, C. K. Shih, M. B. Webb, and M. G. Lagally, Thermal formation of Zn-dopant-vacancy defect complexes on InP(110) surfaces, Phys. Rev. B **53**, 4580, (1996).

[19] P. Ebert, K. Urban, L. Aballe, C. H. Chen, K. Horn, G. Schwarz, J. Neugebauer, and M. Scheffler, Symmetric Versus Nonsymmetric Structure of the Phosphorus Vacancy on InP(110), Phys. Rev. Lett. **84**, 5816 (2000).

[20] C. M. Krammel, M. Roy, F. J. Tilley, P. A. Maksym, L. Y. Zhang, P. Wang, K. Wang, Y. Y. Li, S. M. Wang, and P. M. Koenraad, Incorporation of Bi atoms in InP studied at the atomic scale by cross-sectional scanning tunneling microscopy, Phys. Rev. Mater. **1**, 034606 (2017).

[21] W. Hofer, Challenges and errors: Interpreting high resolution images in scanning tunneling microscopy, Prog. Surf. Sci. **71**, 147 (2003).

[22] J. Tersoff and D. R. Hamann, Theory of the scanning tunneling microscope, Phys. Rev. B **31**, 805 (1985).

[23] G. Kresse and J. Hafner, *Ab initio* molecular dynamics for liquid metals, Phys. Rev. B **47**, 558 (1993).

[24] G. Kresse and J. Furthmuller, Efficient iterative schemes for *ab initio* total-energy calculations using a plane-wave basis set, Phys. Rev. B **54**, 11169 (1996).

[25] J. P. Perdew, K. Burke, and M. Ernzerhof, Generalized Gradient Approximation Made Simple, Phys. Rev. Lett. **77**, 3865 (1996).

[26] A. V. Krukau, O. A. Vydrov, A. F. Izmaylov, and G. E. Scuseria, Influence of the exchange screening parameter on the

performance of screened hybrid functionals, J. Chem. Phys. **125**, 224106 (2006).

[27] C. G. Van de Walle and D. Segev, Microscopic origins of surface states on nitride surfaces, J. Appl. Phys. **101**, 081704 (2007).

[28] M. Bertelli, P. Löptien, M. Wenderoth, A. Rizzi, R. G. Ulbrich, M. C. Righi, A. Ferretti, L. Martin-Samos, C. M. Bertoni, and A. Catellani, Atomic and electronic structure of the nonpolar GaN($1\bar{1}00$) surface, Phys. Rev. B **80**, 115324 (2009).

[29] M. Landmann, E. Rauls, W. G. Schmidt, M. D. Neumann, E. Speiser, and N. Esser, GaN *m*-plane: Atomic structure, surface bands, and optical response, Phys. Rev. B **91**, 035302 (2015).

[30] L. Lymperakis, P. H. Weidlich, H. Eisele, M. Schnedler, J.-P. Nys, B. Grandidier, D. Stiévenard, R. E. Dunin-Borkowski, J. Neugebauer, and P. Ebert, Hidden surface states at nonpolar GaN ($10\bar{1}0$) facets: Intrinsic pinning of nanowires, Appl. Phys. Lett. **103**, 152101 (2013).

[31] The source code for "SEMITIP" and its documentation can be downloaded at http://www.andrew.cmu.edu/user/feenstra/semitip_v5/.

[32] M. C. M. M. van der Wielen, A. J. A. van Roij, and H. vanKempen, Direct Observation of Friedel Oscillations Around Incorporated Si_{Ga} Dopants in GaAs by Low-Temperature Scanning Tunneling Microscopy, Phys. Rev. Lett. **76**, 1075 (1996).

[33] A. P. Wijnheijmer, J. K. Garleff, K. Teichmann, M. Wenderoth, S. Loth, and P. M. Koenraad, Single Si dopants in GaAs studied by scanning tunneling microscopy and spectroscopy, Phys. Rev. B **84**, 125310 (2011).

[34] R. M. Feenstra, Electrostatic potential for a hyperbolic probe tip near a semiconductor, J. Vac. Sci. Technol. B **21**, 2080 (2003).

[35] R. M. Feenstra, Y. Dong, M. P. Semtsiv, and W. T. Masselink, Influence of tip-induced band bending on tunnelling spectra of semiconductor surfaces, Nanotechnology **18**, 044015 (2007).

[36] N. Ishida, K. Sueoka, and R. M. Feenstra, Influence of surface states on tunneling spectra of *n*-type GaAs(110) surfaces, Phys. Rev. B **80**, 075320 (2009).

[37] We could perform STM experiments even at a temperature close to 4 K and obtain tunnel spectra similar to that in Fig. 2(c), indicating that the sample is a degenerate semiconductor.

[38] J. Petalas, S. Logothetidis, S. Boultadakis, M. Alouani, and J. M. Wills, Optical and electronic-structure study of cubic and hexagonal GaN thin films, Phys. Rev. B **52**, 8082 (1995).

[39] Z. Yang and Z. Xu, Electronic and optical properties of unstrained and strained wurtzite GaN, Phys. Rev. B **54**, 17577 (1996).

[40] M. Schnedler, V. Portz, H. Eisele, R. E. Dunin-Borkowski, and P. Ebert, Polarity-dependent pinning of a surface state, Phys. Rev. B **91**, 205309 (2015).

[41] T. R. Albrecht, P. Grütter, D. Horne, and D. Rugar, Frequency modulation detection using high-*q* cantilevers for enhanced force microscope sensitivity, J. Appl. Phys. **69**, 668 (1991).

[42] R. García and R. Pérez, Dynamic atomic force microscopy methods, Surf. Sci. Rep. **47**, 197 (2002).

[43] F. J. Giessibl, Advances in atomic force microscopy, Rev. Mod. Phys. **75**, 949 (2003).

[44] L. Gross, F. Mohn, N. Moll, P. Liljeroth, and G. Meyer, The chemical structure of a molecule resolved by atomic force microscopy, Science **325**, 1110 (2009).

[45] P. Pou, Ó. Custance, P. Jelinek, S. Morita, R. Pérez, and M. Abe, Real topography, atomic relaxations, and short-range chemical interactions in atomic force microscopy: The case of the α-Sn/Si(111)-($\sqrt{3} \times \sqrt{3}$)$r30^o$ surface, Phys. Rev. B **73**, 205329 (2006).

[46] Y. Sugimoto, M. A. Lantz, H. J. Hug, R. Hoffmann, P. J. A. van Schendel, P. Kappenberger, S. Martin, A. Baratoff, and H.-J. Güntherodt, Quantitative measurement of short-range chemical bonding forces, Science **291**, 2580 (2001).

[47] N. Oyabu, P. Pou, Y. Sugimoto, P. Jelinek, M. Abe, S. Morita, R. Pérez, and O. Custance, Single Atomic Contact Adhesion and Dissipation in Dynamic Force Microscopy, Phys. Rev. Lett. **96**, 106101 (2006).

[48] T. An, T. Eguchi, K. Akiyama, and Y. Hasegawa, Atomically resolved imaging by frequency-modulation atomic force microscopy using a quartz length-extension resonator, Appl. Phys. Lett. **87**, 133114 (2005).

[49] All the data displayed in Fig. 3 were measured at a probe and sample temperature of 4.8 K after keeping the lateral position of the probe over the same surface area for a long time to prevent creep between the STM and AFM images.

[50] P. Rahe, R. Bechstein, J. Schütte, F. Ostendorf, and A. Kühnle, Repulsive interaction and contrast inversion in noncontact atomic force microscopy imaging of adsorbates, Phys. Rev. B **77**, 195410 (2008).

[51] B. J. Albers, T. C. Schwendemann, M. Z. Baykara, N. Pilet, M. Liebmann, E. I. Altman, and U. D. Schwarz, Three-dimensional imaging of short-range chemical forces with picometer resolution, Nat. Nanotech. **4**, 307 (2009).

[52] Y. Sugimoto, P. Pou, M. Abe, P. Jelinek, R. Pérez, S. Morita, and O. Custance, Chemical identification of individual surface atoms by atomic force microscopy, Nature (London) **446**, 64 (2007).

[53] Y. Sugimoto, P. Pou, O. Custance, P. Jelinek, M. Abe, R. Pérez, and S. Morita, Complex patterning by vertical interchange atom manipulation using atomic force microscopy, Science **322**, 413 (2008).

[54] D. C. Look, D. C. Reynolds, J. W. Hemsky, J. R. Sizelove, R. L. Jones, and R. J. Molnar, Defect Donor and Acceptor in GaN, Phys. Rev. Lett. **79**, 2273 (1997).

[55] A. O. Evwaraye, S. R. Smith, and S. Elhamri, Optical admittance spectroscopy studies near the band edge of gallium nitride, J. Appl. Phys. **115**, 033706 (2014).

[56] P. Ebert, L. Ivanova, and H. Eisele, Scanning tunneling microscopy on unpinned GaN($1\bar{1}00$) surfaces: Invisibility of valence-band states, Phys. Rev. B **80**, 085316 (2009).